Original Research Report

Influences of implant neck design and implant-abutment joint type on peri-implant bone stress and abutment micromovement: three-dimensional finite element analysis

Yasufumi Yamanishi[1,2], Satoshi Yamaguchi[1,*], Satoshi Imazato[1], Tamaki Nakano[2], Hirofumi Yatani[2]

[1]Department of Biomaterials Science, Osaka University Graduate School of Dentistry, Osaka, Japan

[2]Department of Fixed Prosthodontics, Osaka University Graduate School of Dentistry, Osaka, Japan

Short Title: 3D FEA of two-piece implants

*Corresponding author.

Satoshi Yamaguchi, PhD

Assistant Professor

Department of Biomaterials Science

Osaka University Graduate School of Dentistry

1-8 Yamadaoka, Suita 565-0871, Japan

Tel: +81-6-6879-2919, Fax: +91-6-6879-2919.

E-mail: yamagu@dent.osaka-u.ac.jp

Objectives. Occlusal overloading is one of the causes of peri-implant bone resorption, and many studies on stress distribution in the peri-implant bone by three-dimensional finite element analysis (3D FEA) have been performed. However, the FEA models previously reported were simplified and far from representing what occurs in clinical situations. In this study, 3D FEA was conducted with simulation of the complex structure of dental implants, and the influences of neck design and connections with an abutment on peri-implant bone stress and abutment micromovement were investigated.

Methods. Three types of two-piece implant CAD models were designed: external joint with a conical tapered neck (EJ), internal joint with a straight neck (IJ), and conical joint with a reverse conical neck (CJ). 3D FEA was performed with the setting of a “contact” condition at the component interface, and stress distribution in the peri-implant bone and abutment micromovement were analyzed.

Results. Among the three groups, EJ had the highest shear stress concentrated on the mesio-distal side of the cortical bone and largest amount of abutment micromovement. While the von Mises and shear stresses around the implant neck were concentrated on the labial bone for EJ, they were distributed on the mesiodistal side of the cortical bone for CJ. CJ had the least amount of abutment micromovement.

Significance. Implants with a conical joint with an abutment and reverse conical neck design may effectively control occlusal overloading on the labial bone and abutment micromovement.

Keywords: biomechanics, dental implant, finite element analysis, occlusal force, micromovement

1. Introduction

In accordance with the increase in their success rate, dental implants have become a popular treatment option for missing teeth. One of the criteria for successful dental implant treatment is radiographic vertical peri-implant bone loss of <2.0 mm [1]. Remodeling of the peri-implant bone occurs once the implant is exposed to the oral environment by a second surgical procedure or by the immediate placement of an abutment after implant surgery. Factors that negatively affect the remodeling process and result in marginal bone resorption include traumatic surgical technique [2], excessive loading conditions [3], microbial contamination of the microgap between an implant and an abutment [4-6], micromovement of an implant and abutment [4,7-9], and repeated screwing and unscrewing [10]. Exclusion of one or more of these factors is important for successful implant treatment.

Osteoclastic bone resorption occurs in areas where microcracks are produced by occlusal dynamic stress and osteocyte apoptosis [11,12]. Bone is resistant to compressive stress but is susceptible to tensile and shear stresses, and the threshold values of tensile and shear stresses that cause resorption of cortical bone are reportedly about 30% and 65% less than the threshold value of compressive stress, respectively [13,14]. Therefore, reducing the shear stress caused by occlusal loading effectively

controls peri-implant bone resorption [14]. Considering the benefits of eliminating an excessive occlusal loading condition [15-20], much attention has been paid to biomechanical evaluation of implants. Finite element analysis (FEA) is useful for numerical stress analysis of multiple structured materials and has been widely used for the analysis of dental implants. However, because dental implants have a complex structure, most of the previous FEA studies utilized simplified simulation such as two-dimensional models [15,16] or three-dimensional (3D) models of one-piece implants coupled with an abutment [17-19]. While advantageous in terms of calculation costs, limited information on stress distribution can be provided by two-dimensional models. The 3D models are more informative and clinically relevant. However, one-piece models do not reflect the real structure of implants, and stress distribution analysis of each component of an implant is not possible.

In this study, 3D two-piece implant CAD models were created, and FEA was performed by a CAD software add-in. In addition, different implant body and abutment connection types were designed, including the reverse conical neck by which bone platform switching [21] is achieved. The purpose of this study was to investigate the influences of the neck design of an implant body and types of implant-abutment joints on peri-implant bone stress by 3D FEA of two-piece structured implants. Under

simulation of the complex structure of implants, the influences of these designs on stress in the abutment screw and abutment micromovement were also evaluated.

2. Materials and methods

2.1. 3D CAD model

Three 3D models were created by CAD functions in computer-aided engineering software (SolidWorks Simulation 2011; SolidWorks Corporation, MA, USA) (Fig. 1A-C). The diameter and length of the implant body, the shape of the neck, and the types of implant-abutment joints of the three models are shown in Table 1. The pitch and shape of the threads were the same in all groups. Each abutment had the same shape and size with the exception of the type of connection with the implant body. The implant and abutment were connected with an abutment screw.

A CAD model of an anterior maxillary bone with a 1.5-mm-wide cortical bone was prepared, and each 3D implant model was placed (Fig. 1D). The mechanical properties of bone and titanium used for the finite element (FE) models are shown in Table 2 [22]. For simulations of osseointegrated implants, a “fixed bond” condition was set at the interface of the bone and the implant. A “contact” condition, which accepts possible microscopic sliding, was set at the interfaces among the components of the implants. The bottom part of the maxillary bone was fixed, and a static load of 100 N was applied to the basal ridge surface of the abutment 45° obliquely to the long axis of the implant (Fig. 1E). Elements for FEA were tetrahedrons. The results of convergence

testing to select the best number of elements are shown in Table 3. FEA was performed by SolidWorks Simulation SolidWorks 2011 add-in (SolidWorks Corporation).

2.2. Peri-implant bone stress

By FEA, distributions of the principal, shear, and von Mises stresses in the peri-implant bone were assessed. The value of the maximum principal stress was recorded.

2.3. Strain distribution in abutment screw

Distribution of the equivalent strain in the abutment screw was assessed by FEA. In the middle section of mesiodistal plane, the equivalent strain distribution was determined.

2.4. Micromovement of abutment

In the mesiodistal plane, distribution of the principal stress on the abutment in the x-axis direction and shear stress at the interface of the implant and the abutment in the y-axis direction were assessed. Micromovement of the abutment was calculated from the volume before (V_{before}) and after displacement (V_{after}) using the following

equation:

$$\text{Micromovement} = \frac{V_{after} - \left(V_{before} \cap V_{after}\right)}{V_{before} \cup V_{after}} \times 100 \quad (\%)$$

3. Results

3.1. Peri-implant bone stress

Fig. 2 shows the principal stress distribution in the peri-implant bone. In all models, the principal stress was concentrated on the bone around the implant neck. For CJ, the principal stress concentration was found in the mesiodistal side.

Distribution of von Mises stress around the implant neck and shear stress in the z-axis direction (xz-plane) around the first thread of the implant body for IJ and CJ are shown in Fig. 3. For IJ, the von Mises stress was concentrated on the labial bone around the implant neck, and intense concentration of shear stress around the first thread on the labial side was observed (Fig. 3A, B). On the contrary, the von Mises and shear stresses were distributed in the mesiodistal direction for CJ (Fig. 3C, D).

Fig. 4 shows the principal stress in the x-axis direction and the shear stress in the y-axis direction in the peri-implant cortical bone. For EJ, the boundary between the compressive and tensile stresses was clearly seen on the mesiodistal side of the cortical bone (Fig. 4A), and the shear stress was concentrated on the mesiodistal side of the cortical bone (Fig. 4B). On the contrary, for IJ and CJ, the boundary of the principal stress was not clear and the shear stress concentration on the cortical bone was small.

The maximum principal stress value in the bone was in the order EJ < IJ < CJ (Table 4).

3.2. Strain in abutment screw

Fig. 5 shows the distribution of the equivalent strain in the abutment screw for each model. The strain was concentrated on the top and middle of the screw for EJ, while IJ and CJ exhibited uniform distribution of the strain on the palatal side.

3.3. Micromovement of abutment

Fig. 6 shows the distribution of the principal stress in the x-axis direction of the abutment and the shear stress in the y-axis direction at the interface between the implant and the abutment. For EJ, the principal stress was concentrated on the inside palatal surface of the abutment (Fig. 6A), indicating that the abutment screw was bent and that compressive stress in the x-axis direction was generated. The distribution of the shear stress in the same direction was identical for IJ. However, for CJ, the interface was subjected to shear stress in the opposite direction (Fig. 6B).

Abutment micromovement in percentage per unit volume was in the order EJ > IJ > CJ (Table 5).

4. Discussion

FEA is a useful tool with which to predict the longevity of restorative and prosthetic treatments under simulation of loading conditions in the oral environment [23]. Severe peri-implant bone resorption was reportedly found around two-piece implants because of abutment micromovement and microgap formation between the implant and the abutment [4,8,9]. To obtain clinically relevant information on the stress distribution related to bone loss and within implant components, FEA with models that simulate the detailed structure of implants is indispensable. In this study, we created 3D CAD models of two-piece implants and performed the analysis in a more realistic fashion than previously reported. FEA is time-consuming and calculation costs are expensive when complex-structured materials are analyzed. SolidWorks Simulation software containing FEA add-in is useful not only for 3D CAD, but also for the analysis. Using this software, we successfully evaluated the stress in the peri-implant bone and implant components in three dimensions, comparing the different implant-abutment connection types.

Depending on the hardness of foods, the average bite force reportedly ranges from 20 to 120 N [24]. In the present study, we applied a static load of 100 N to simulate loading by occlusion in reference to some previous studies [25,26]. The

principal stress concentration in the bone for the two-piece implant occurred around the neck, similar to the previous reports that demonstrated stress concentration around the neck of one-piece implant models [17-19,25]. For EJ, the boundary between the compressive and tensile stresses was clearly shown on the mesiodistal side of the cortical bone. This result indicates that the shear stress on the peri-implant bone in the direction of the y-axis was concentrated on the mesiodistal side of the cortical bone for EJ. Bone has lower resistance to shear stress compared with tensile or compressive stresses, and shear stress appears to play an important role in the resorption of cortical bone [13,14]. Therefore, it is considered that an external joint with an abutment influences proximal bone resorption. For IJ with a straight neck, the von Mises stress was concentrated on the labial bone around the implant neck, and intense concentration of shear stress in the labial bone around the first thread of the implant was observed. On the contrary, for CJ with a reverse conical neck, the principal stress concentration was found on the mesiodistal side, and the von Mises and shear stresses in the labial bone around the implant neck were less concentrated than those for IJ. These results suggest that the reverse conical neck design influences peri-implant bone stress distribution. Bone platform switching results in an inward bone ring in the coronal part of an implant that is in continuity with the alveolar bone crest [21]. Therefore, the reverse conical

neck design may be useful to control labial bone resorption compared with the straight neck design.

Maximum stress values have been determined in many mechanical stress analyses of dental implants [8,9,15,16,18,19,25,27]. Among the three models, the maximum principal stress value in the bone was the greatest for CJ. It is suggested that the deep, rigid connections of IJ and CJ with an implant are sensitive to the stress distribution and transmit the load more directly to the bone around the implant neck.

The 3D two-piece models fabricated in the present study were useful to evaluate the stress in the implant components in three dimensions. For rigid connections with an abutment (i.e., IJ and CJ), the equivalent strain of the abutment screw was uniformly distributed. On the other hand, for flexible connections with an abutment (i.e., EJ), concentration of the equivalent strain occurred in the middle and top of the abutment. In addition, for EJ, the compressive stress in the x-axis direction was concentrated on the inside palatal surface of the abutment. It is considered that the abutment screw of EJ bends greatly and slides microscopically by repeated occlusal stress, suggesting that the abutment screw of EJ may loosen more easily. For IJ, the distribution of the shear stress in the y-axis direction of the interface between the implant and the abutment was uniformly dispersed. However, for CJ, the shear stress in

the opposite direction occurred at the interface between the implant and the abutment. This suggests that the taper of the abutment of CJ resists microscopic sliding between the implant and the abutment.

In addition to negative influences on peri-implant bone remodeling [28], abutment micromovement may also induce destruction of the epithelial attachment to the abutment and crown and result in bacterial microleakage [10,29]. In this study, we successfully simulated micromovement and assessed the effects of different connection types by means of two-piece implant CAD models. The amount of micromovement in the three models was in the order EJ > IJ > CJ, and EJ with a flexible connection exhibited the greatest movement. This finding can be explained by the large amount of bending of the abutment screw and the fact that the compressive stress of the abutment in the x-axis direction was concentrated on the inside palatal surface for EJ.

The results of the present FEA study revealed that neck design and abutment connection types affect stresses generated in the bone and abutment micromovement. Therefore, use of an implant with the least stress generation and abutment micromovement may be recommended to reduce peri-implant bone resorption. Optimization of implant design by further analysis with detailed simulation of the structure of clinically used implants could help to exclude overload and subsequently

achieve a better prognosis.

5. Conclusions

Implant neck design and implant-abutment joint types influence peri-implant bone stresses and abutment micromovement. The reverse conical neck design and conical joint implants with an abutment are recommended to reduce occlusal stress concentration on the labial bone and abutment micromovement. Abutments of external joint implants might loosen more easily, while tapered abutments are more resistant to loosening.

Acknowledgment

This research was supported by Grants-in-Aid for Scientific Research (21791938 and 23390434) from the Japan Society for the Promotion of Science (JSPS).

References

1. Misch CE, Perel ML, Wang HL, Sammartino G, Galindo-Moreno P, Trisi P, Steigmann M, Rebaudi A, Palti A, Pikos MA, Schwartz-Arad D, Choukroun J, Gutierrez-Perez JL, Marenzi G and Valavanis DK. Implant success, survival, and failure: the International Congress of Oral Implantologists (ICOI) Pisa Consensus Conference. Implant Dent, 2008; 17:5-15.

2. Becker W and Goldstein M. Minimally invasive flapless implant surgery: a prospective multicenter study. Clin Implant Dent Relat Res, 2005; 7 Suppl. 1:S21-S27.

3. Kim Y and Oh TJ. Occlusal considerations in implant therapy: clinical guidelines with biomechanical rationale. Clin Oral Implants Res, 2005; 16:26-35.

4. Hermann JS and Schoolfield JD. Influence of the size of the microgap on crestal bone changes around titanium implants. A histometric evaluation of unloaded non-submerged implants in the canine mandible. J Periodontol, 2001; 72:1372-1383.

5. Weng D and Nagata MJ. Influence of microgap location and configuration on the periimplant bone morphology in submerged implants. An experimental study in dogs. Clin Oral Implants Res, 2008; 19:1141-1147.

6. Ericsson I and Persson LG. Different types of inflammatory reactions in peri-implant soft tissues. J Clin Periodontol, 1995; 22:255-261.

7. King GN and Hermann JS. Influence of the size of the microgap on crestal bone levels in non-submerged dental implants: a radiographic study in the canine mandible. J Periodontol, 2002; 73:1111-1117.

8. Weng D, Nagata MJH, Bosco AF and Melo LGN. Infuence of microgap location and configuration on radiographic bone loss around submerged implants: an experimental study in dogs. Int J Oral Maxillofac Implants, 2011; 26(5):941-946.

9. Hermann JS, Schoolfield JD, Scenk RK, Buser D and Cochran DL. Influence of the size of the microgap on crestal bone changes around titanium implants. A histometric evaluation of unloaded non-submerged implants in the canine mandible. J Periodontol,

2001; 72(10):1372-1383.

10. Abrahamsson I and Berglundh T. The mucosal barrier following abutment dis/reconnection. An experimental study in dogs. J Clin Periodontol, 1997; 24:568-572.

11. Verborgt O, Gibson GJ and Schaffler MB. Loss of osteocyte integrity in association with microdamage and bone remodeling after fatigue in vivo. J Bone Miner Res, 2000; 15:60-67.

12. Huiskes R and Ruimerman R. Effect of mechanical forces on maintenance and adaptation of form in trabecular bone. Nature, 2000; 405:704-706.

13. Reilly DT and Burstein AH. The elastic and ultimate properties of compact bone tissue. J Biomech, 1975; 8:393-405.

14. Guo XE. Mechanical properties of cortical bone and cancellous bone tissue. In: Cowin SC, ed. Bone Mechanics Handbook; 2001. pp. 1-23.

15. Schrotenboer J and Tsao YP. Effect of microthreads and platform switching on crestal bone stress levels: a finite analysis. J Periodontol, 2008; 79:2166-2172.

16. Schrotenboer J, Tsao YP, Kinariwala V and Wang HL. Effect of platform switching on implant crest bone stress: a finite element analysis. Implant Dent, 2009; 18:260-269.

17. Petrie CS and Williams JL. Comparative evaluation of implant designs: influence of diameter, length, and taper on stains in the alveolar crest. A three-dimensional finite-element analysis. Clin Oral Implants Res, 2005; 16:486-494.

18. Hudieb MI, Wakabayashi N and Kasugai S. Magnitude and direction of mechanical stress at the osseointegrated interface of the microthread implant. J Periodontol, 2011; 82:1061-1070.

19. Chang CL, Chen CS and Hsu ML. Biomechanical effect of platform switching in implant dentistry: a three-dimensional finite analysis. Int J Oral Maxillofac Implants, 2010; 25:295-304.

20. Hsu JT, Fuh LJ, Lin DJ, Shen YW and Huang HL. Bone strain and interfacial sliding analyses of platform switching and implant diameter on an immediately loaded implant: experimental and three-dimensional finite element analysis. J Periodontol, 2009; 80:1125-1132.

21. Danza M and Carinci F. Bone platform switching: a retrospective study on the slope of reverse conical neck. Quintessence Int, 2010; 41:35-40.

22. Pessoa RS, Vaz LG, Marcantonio E Jr, Vander Sloten J, Duyck J and Jaecques SV. Biomechanical evaluations of platform switching in different implant protocols: computed tomography-based three-dimensional finite element analysis. Int J Oral Maxillofac Implants, 2010; 25(5):911-919.

23. Farah JW, Craig RG. Finite element stress analysis of a restored axisymmetric first molar. J Dent Res, 1974; 53(4):859-866.

24. Dittmer S, Dittmer MP, Kohorst P, Jendras M, Borchers L and Stiesch M. Effect of implant-abutment connection design on load bearing capacity and failure mode of implants. J Prosthodont, 2011; 20(7):510-516.

25. Tabata LF, Rocha EP, Barao VA and Assuncao WG. Platform switching: biomechanical evaluation using three-dimensional finite element analysis. Int J Oral Maxillofac Implants, 2011; 26(3):482-491.

26. Natali AN, Pavan PG and Ruggero AL. Analysis of bone-implant interaction phenomena by using a numerical approach. Clin Oral Implants Res, 2006; 17(1):67-74.

27. Assuncao WG, Gomes EA, Barao VA and de Sousa EA. Stress analysis in simulation models with or without implant threads representation. Int J Oral Maxillofac Implants, 2009; 24(6):1040-1044.

28. Atieh MA, Ibrahim HM and Atieh AH. Platform switching for marginal bone preservation around dental implants: a systematic review and meta-analysis. J Periodontol, 2010; 81:1350-1366.

29. Steinebrunner L, Wolfart S, Bobmann K, Kern M. In vitro evaluation of bacterial leakage along the implant-abutment interface of different implant systems. Int J Oral Maxillofac Implants, 2005; 20(6):875-881.

Figures

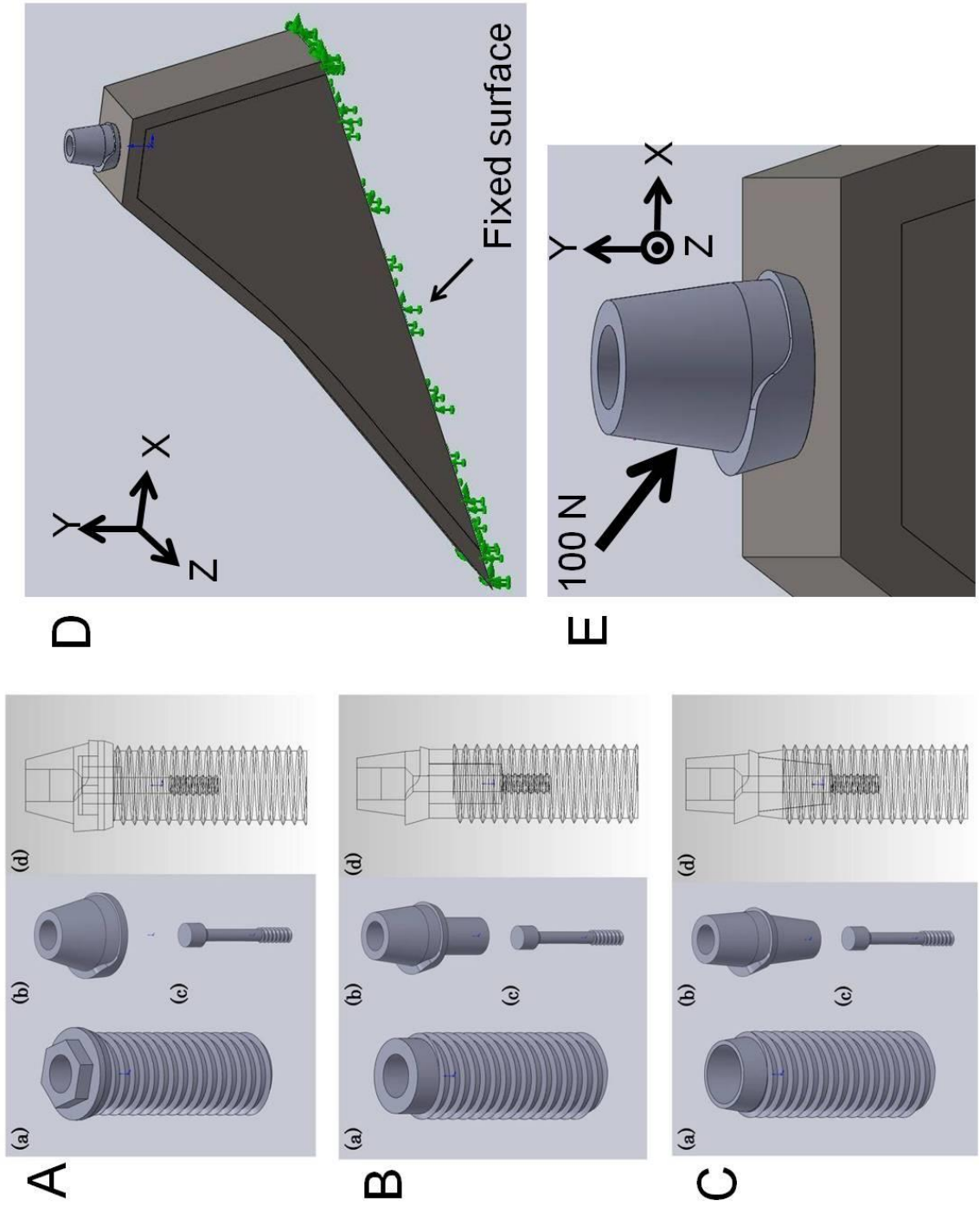

Fig. 1

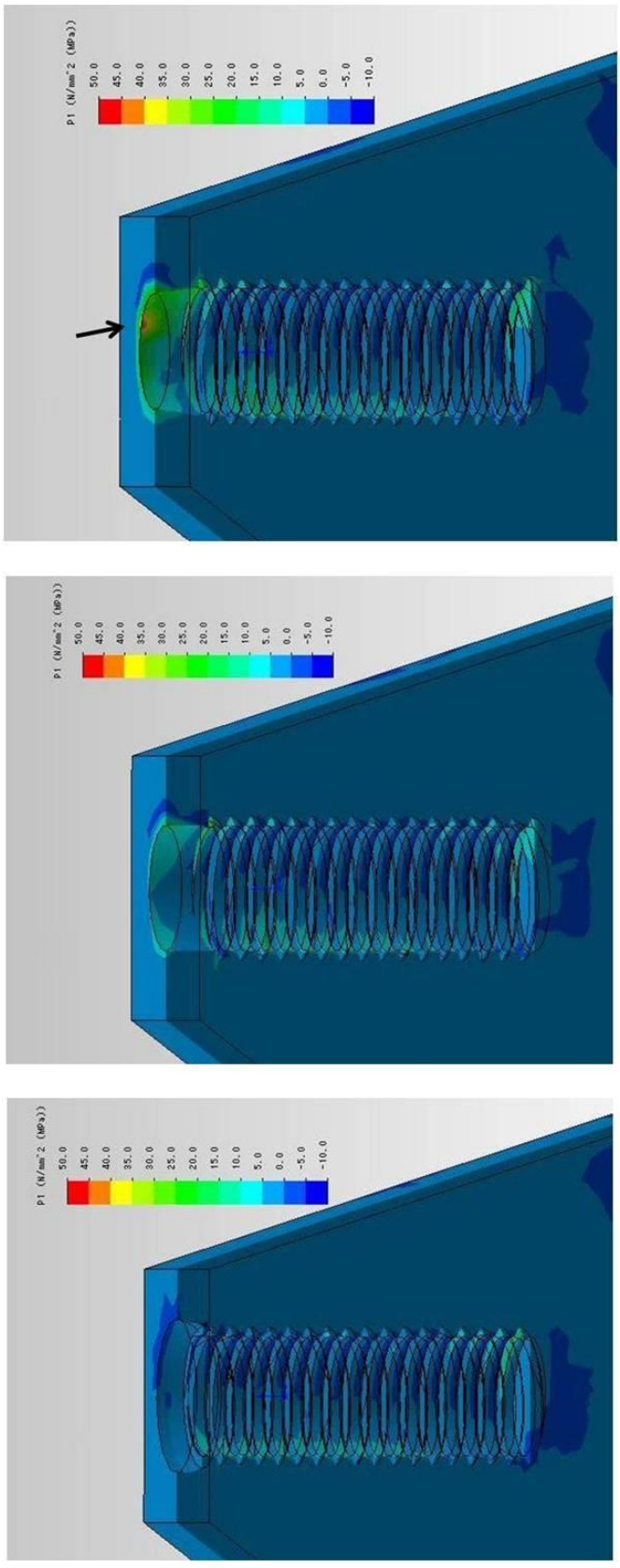

Fig. 2

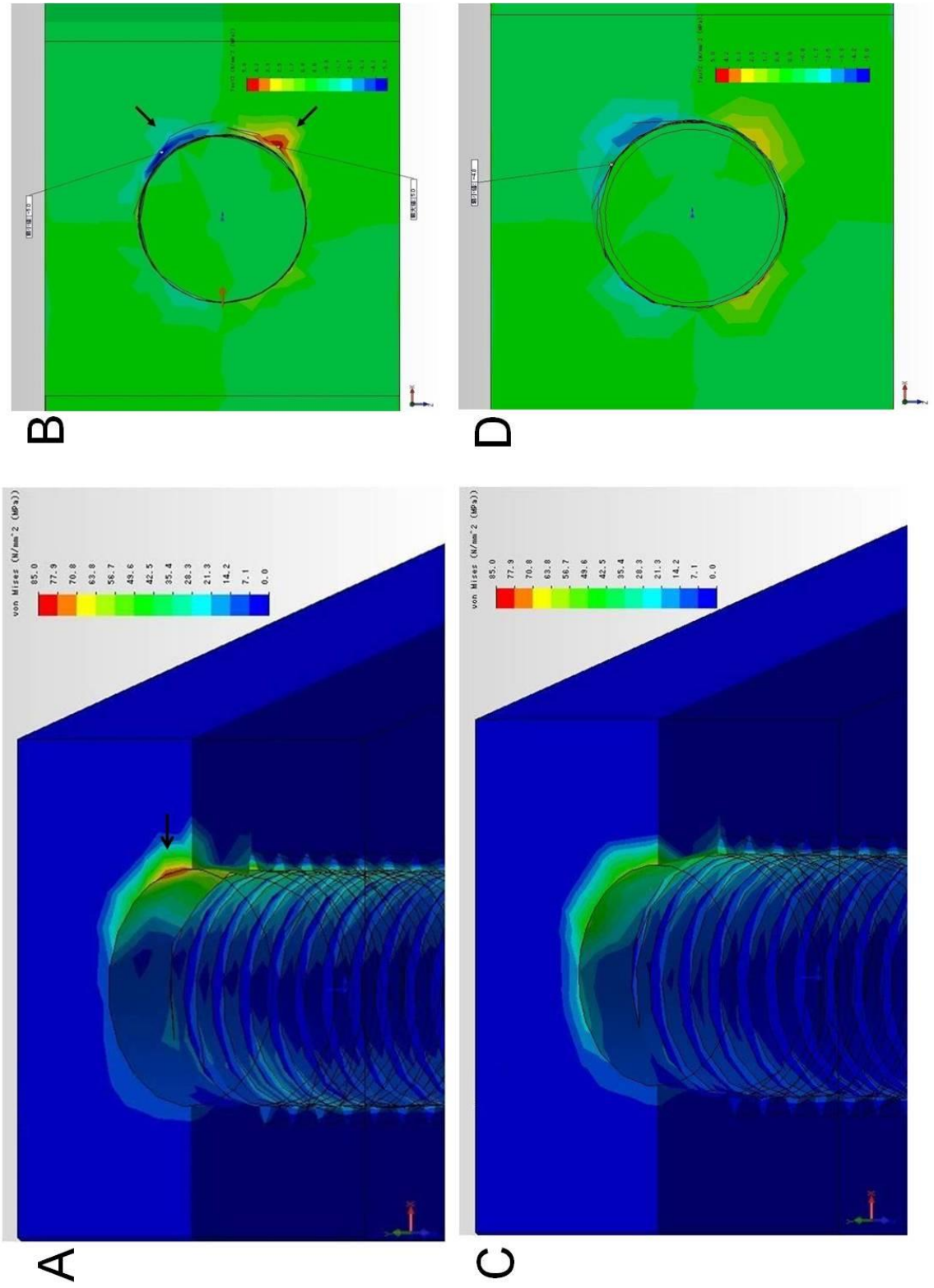
B
D
A
C
von Mises (N/mm^2 (MPa))
85.0
77.9
70.8
63.8
56.7
49.6
42.5
35.4
28.3
21.3
14.2
7.1
0.0

Fig. 3

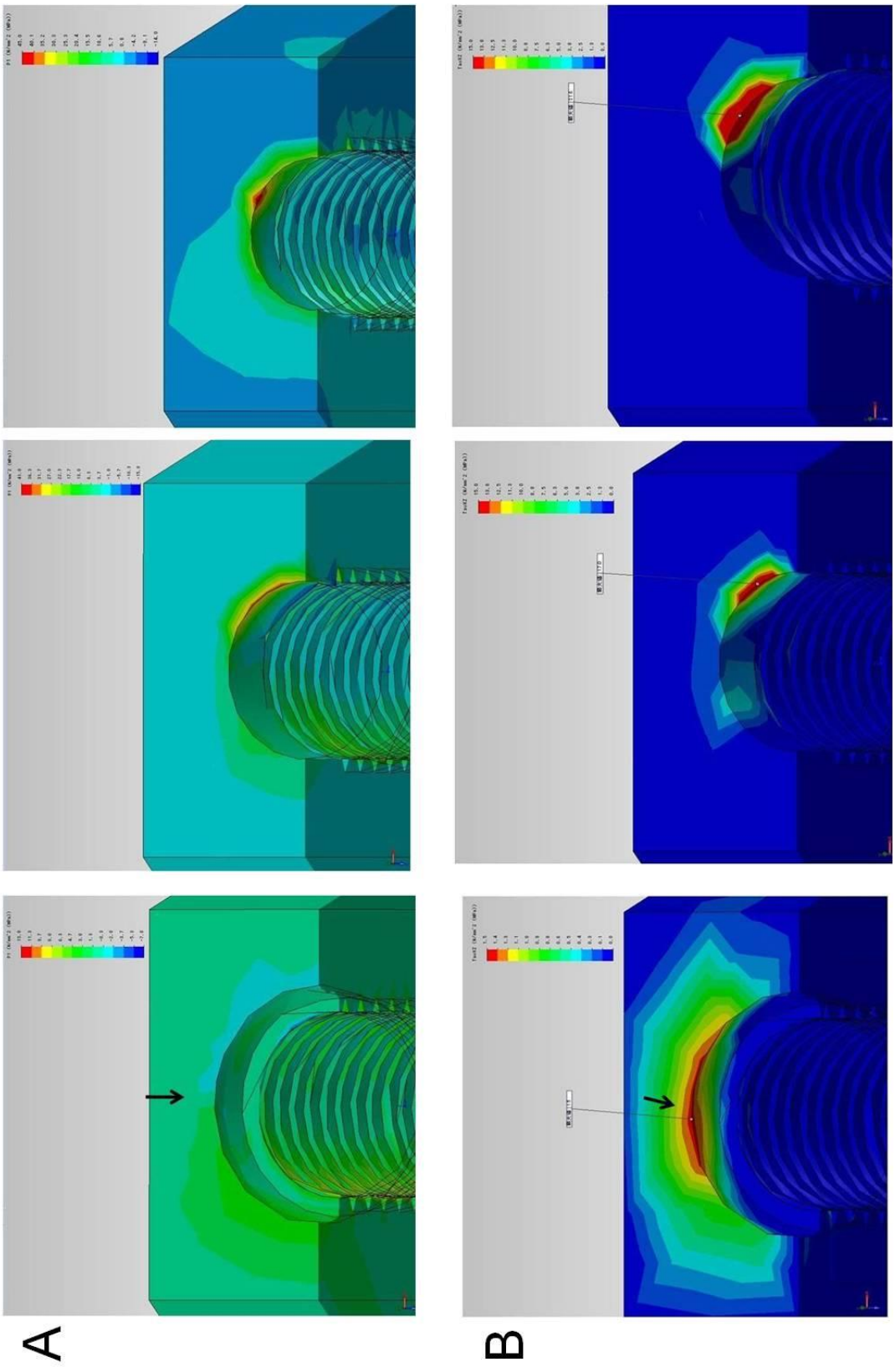

Fig. 4

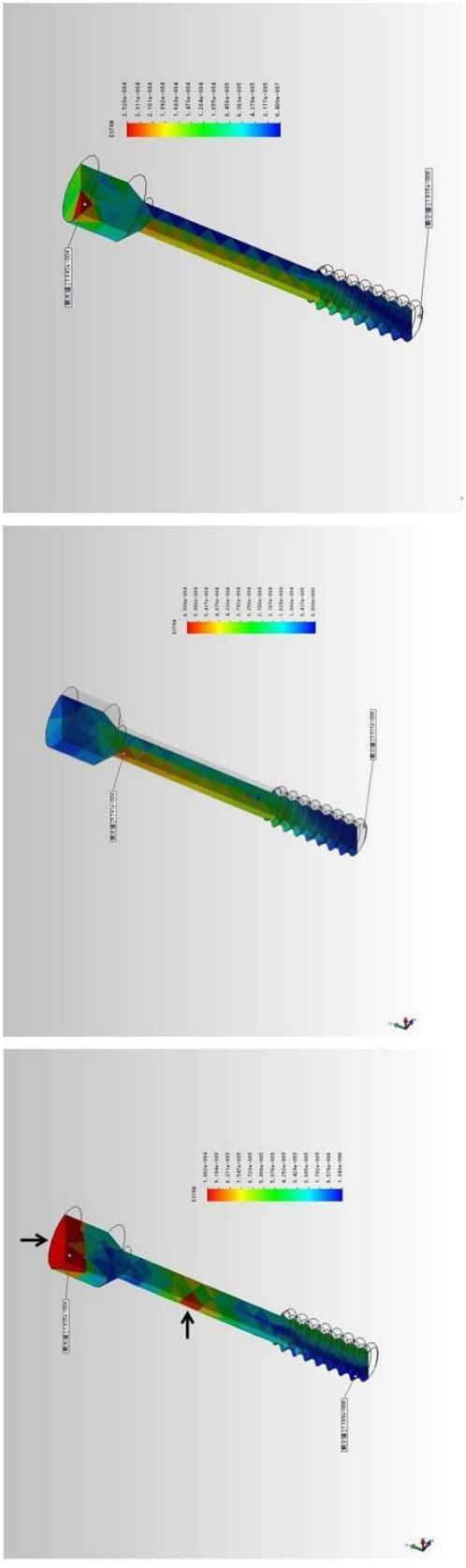

Fig. 5

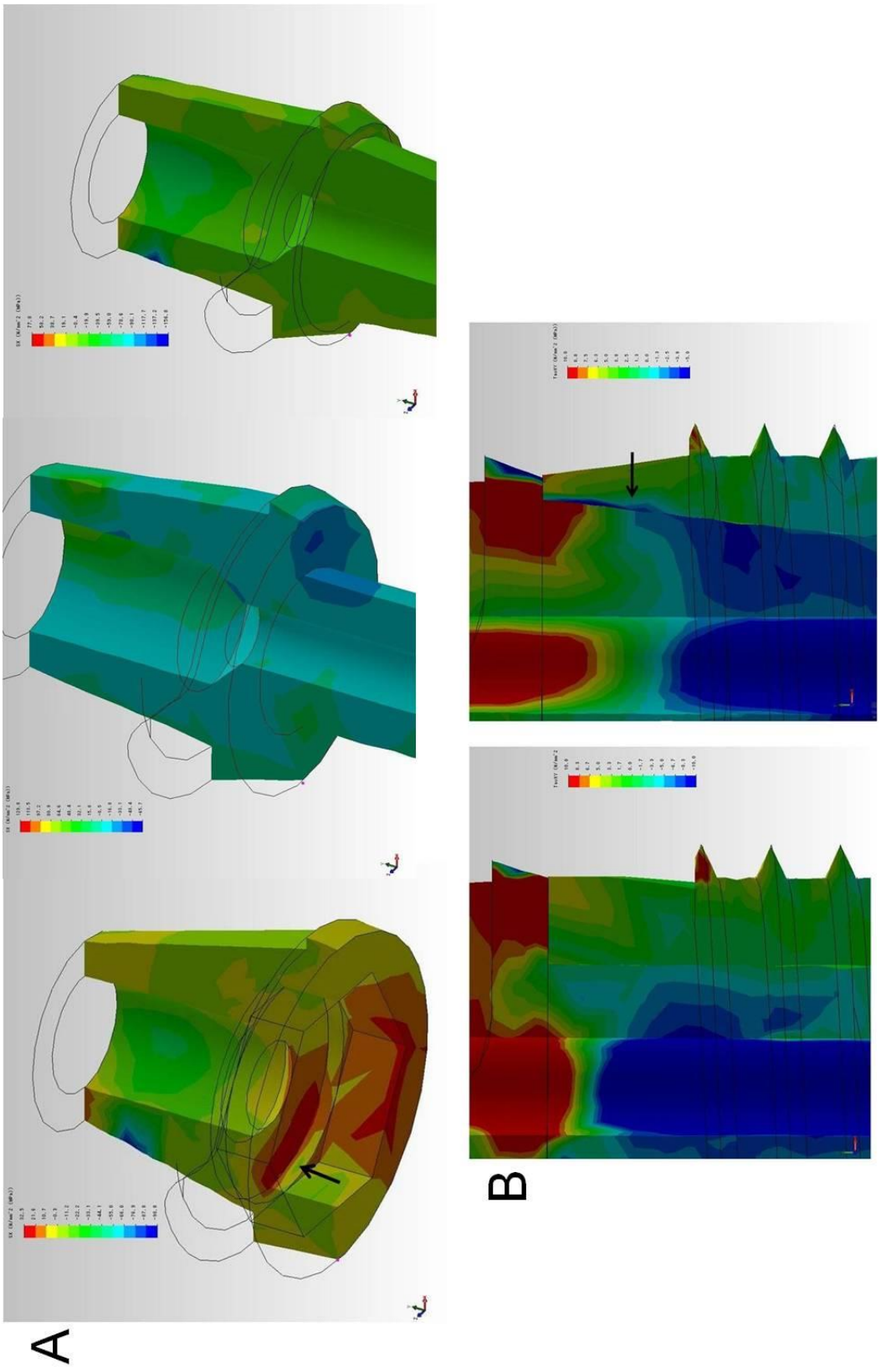

Fig. 6

Captions

Table 1. Three-dimensional CAD models

Table 2. Mechanical properties of bone and titanium used for FEA

Table 3. Total number of elements and nodes for each model

Table 4. Maximum principal stress value for each model (MPa)

Table 5. Micromovement of the abutment (%)

Figure 1. Three-dimensional CAD models (A, B, C) and views of the finite element model (D, E).

(A) EJ, (B) IJ, (C) CJ. (a) Implant body, (b) abutment, (c) abutment screw, (d) connected body.

(D) Whole assembly of bone and implant models. The bottom part of the bone was fixed.

(E) Static load of 100 N was applied to the basal ridge surface of the abutment 45° obliquely to the long axis of the implant.

Figure 2. Maximum principal stress distributions for EJ (left), IJ (center), and CJ (right). Black arrow indicates the concentration of principal stress on the mesiodistal side of the peri-implant bone.

Figure 3. The von Mises stress distribution around the implant neck (A, C) and the shear stress distribution around the first thread of the implant (B, D).

(A, B) IJ, (C, D) CJ.

Black arrows indicate concentrations of von Mises and shear stresses.

Figure 4. Distributions of the principal and shear stresses.

(A) Principal stress distributions on the proximal side of the peri-implant bone for EJ (left), IJ (center), and CJ (right).

Black arrow shows the boundary between the compressive and tensile stresses.

(B) Shear stress distributions on the proximal side of the peri-implant bone for EJ (left), IJ (center), and CJ (right).

Black arrow shows the concentration of shear stress.

Figure 5. Equivalent strain distributions in an abutment screw for EJ (left), IJ (center), and CJ (right).

Black arrows show that the strain was concentrated on the top and middle of the screw.

Figure 6. Distribution of principal and shear stresses.

(A) Principal stress distributions of an abutment for EJ (left), IJ (center), and CJ (right).

Black arrow shows that the principal stress in the direction of x-axis was concentrated on the inside palatal surface of the abutment.

(B) Shear stress distributions of the interface between an implant and an abutment for IJ (left) and CJ (right).

Black arrow shows that the interface was subject to opposite shear stress.